Homo- and Heterometallic [2×2] Grid Arrays Containing Ru^{II}, Os^{II}, and Fe^{II} Subunits and their Mononuclear Ru^{II} and Os^{II} Precursors: Synthesis, Absorption Spectra, Redox Behavior, and Luminescence Properties

Dario M. Bassani,[a, b] Jean-Marie Lehn,*[a] Scolastica Serroni,[c] Fausto Puntoriero,[c] and Sebastiano Campagna*[c]

Abstract: The absorption spectra, redox behavior, and luminescence properties (both at 77 K in rigid matrices and at room temperature in fluid solution) of a series of [2×2] molecular grids have been investigated. The latter were prepared either by means of sequential self-assembly, or by a stepwise protection/deprotection procedure, and are based on a ditopic hexadentate ligand **1** in which two terpyridine-like binding sites are fused together in a linear arrangement. The molecular grids studied include the homometallic species $[\{Fe(\mathbf{1})\}_4]^{8+}$ (**Fe_2Fe_2**), and the heterometallic species $[\{Ru(\mathbf{1})\}_2\{Fe(\mathbf{1})\}_2]^{8+}$ (**Ru_2Fe_2**) and $[\{Os(\mathbf{1})\}_2\{Fe(\mathbf{1})\}_2]^{8+}$ (**Os_2Fe_2**). For comparison purposes, the properties of the mononuclear complexes $[Ru(\mathbf{1})_2]^{2+}$ (**1-Ru**) and $[Os(\mathbf{1})_2]^{2+}$ (**1-Os**) have been studied. All these compounds exhibit very intense absorption bands in the UV region (ε in the 10^5–$10^6\,M^{-1}\,cm^{-1}$ range, attributed to spin-allowed ligand-centered (LC) transitions), as well as intense metal-to-ligand charge-transfer (MLCT) transitions (ε in the 10^4–$10^5\,M^{-1}\,cm^{-1}$ range) that extend to the entire visible region. The mononuclear species **1-Ru** and **1-Os** exhibit relatively intense luminescence, both in acetonitrile at room temperature (τ = 59 and 18 ns, respectively) and in butyronitrile rigid matrices at 77 K. In contrast, the tetranuclear molecular grids do not exhibit any luminescence, either at room temperature or at 77 K. This is attributed to fast intercomponent energy transfer from the Ru- or Os-based subunits to the low-lying metal-centered (MC) levels involving the Fe^{II} centers, which leads to fast radiationless decay. The redox behavior of the compounds is characterized by several metal-centered oxidation and ligand-centered reduction processes, most of them reversible in nature (as many as twelve for **Fe_2Fe_2**). Detailed assignment of each redox process has been made, and it is apparent that these systems can be viewed as multilevel molecular electronic species capable of reversibly exchanging a number of electrons at accessible and predetermined potentials. Furthermore, it is shown that the electronic interaction between specific subunits depends on their location in the structure and on the oxidation states of the other components.

Keywords: cyclic voltammetry · fluorescence spectroscopy · grid-type complexes · N ligands · self-assembly

Introduction

The development of nanoscale molecular and supramolecular devices incorporating photo- and electro-active centers has emerged as a viable route to smart functional materials operating at the molecular level.[1–3] Supramolecular self-assembly has played a major role in the move from isolated molecules to complex, interactive ensembles, and a wide variety of well-defined supramolecular architectures have been prepared to date.[3,4] A major feature of the self-assembly process is that individual components will spontaneously combine in a pre-determined fashion due to the presence of complementary molecular recognition sites, thus offering efficient access to nanometer-sized assemblies. The construction of metallo-supramolecular architectures in which metal ions are spatially arranged in two-dimensional grid arrays is

[a] Prof. Dr. J.-M. Lehn, Dr. D. M. Bassani
ISIS, Université Louis Pasteur
CNRS UMR 7006, BP 70028, 67083 Strasbourg (France)
Fax: (+33) 390-24-5140
E-mail: lehn@isis.u-strasbg.fr

[b] Dr. D. M. Bassani
Current address: LCOO, Université Bordeaux I
CNRS UMR 5802, 33405 Talence (France)

[c] Prof. Dr. S. Campagna, Dr. S. Serroni, Dr. F. Puntoriero
Dip. Chimica Inorg. e Strut. Molecol. Univ. Messina
Via Sperone, 31, 98166 Messina (Italy)
Fax: (+39) 090-393-756
E-mail: photochem@chem.unime.it

© 2003 Wiley-VCH Verlag GmbH & Co. KGaA, Weinheim
DOI: 10.1002/chem.200305441

particularly interesting in view of their electro-optical and magnetic properties.[5,6] An additional feature of these assemblies is the possibility of directing their deposition onto solid substrates through secondary molecular recognition motifs, such as hydrogen bonding.[7a,b] In light of this, the design of advanced grid-type architectures containing different metal ions localized in a specific arrangement represents a significant step forward in the development of functional molecular devices.

Previous examples of well-defined supramolecular structures that contained different metal ions relied on the use of different binding sites, each adapted to a particular metal ion.[8] The combination of binding sites and their spatial arrangement can be viewed as a molecular program, to be read-out by the metal ions through their coordination features during the self-assembly process. This approach has recently made it possible to direct the formation of highly functionalized assemblies combining helical and grid-like sub-structures.[8b,c] It relies on the use of metal ions that possess different coordination geometries coupled to the use of specially designed ligands to direct the self-assembly process. A complementary approach makes use of metal ions of like coordination geometry, but of different kinetic stability to construct complex architectures in a step-wise manner.

The mixed-metal complexes described in this study are based on the ditopic hexadentate ligand **1**, in which two terpyridine-like binding sites are fused together in a linear arrangement (Scheme 1). In principle, whereas the construction of a homometallic [2×2] grid can only lead to one structure, the incorporation of two different metal ions during the assembly produces grid-type structures that may exist as either *anti* or *syn* topoisomers (localization isomers). When both ions possess identical coordination spheres, a sequential self-assembly strategy must be employed to direct the formation of only one isomer. For this to be effective, the second metal ion to be introduced must be of lower kinetic stability than the first, allowing the use of milder reaction conditions to avoid scrambling with the metal centers already present. We have previously reported the successful use of this approach to prepare mixed-metal grids combining the kinetically inert Ru^{II} or Os^{II} with a second metal ion (Fe^{II}, Co^{II}, or Ni^{II}).[9] The investigation of the spectroscopic, redox, and luminescence properties of the multimetallic structures described here provides new information concerning the intra-assembly through-space and through-ligand metal–metal interactions, ligand–ligand interactions mediated by the metal centers, and the occurrence of photoinduced energy-transfer processes within the grid structures. A schematic representation of all the species investigated here is shown in Figure 1.

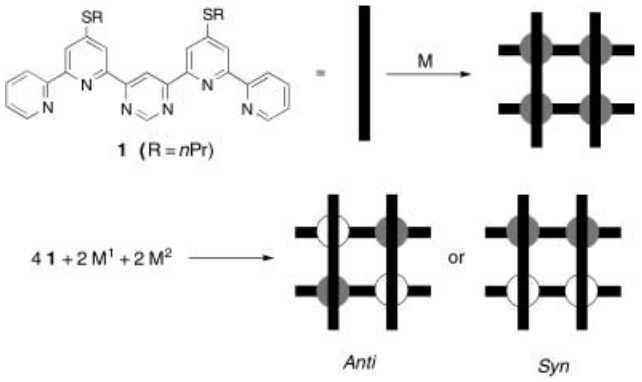

Scheme 1. Schematic representation of the homometallic and heterometallic tetranuclear [2×2] grid structures obtained from ligand **1**.

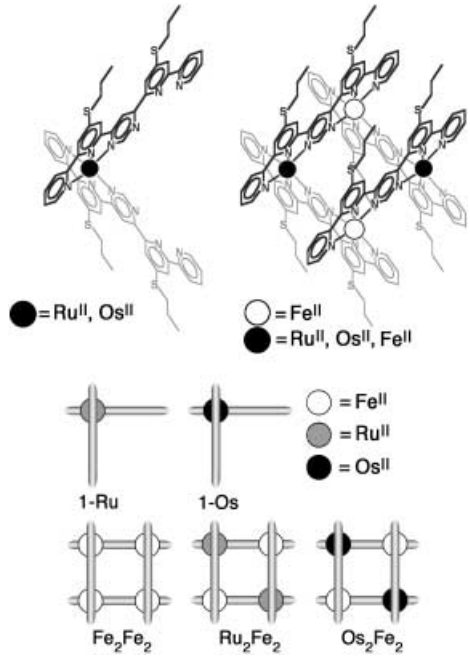

Figure 1. Structural formulae and schematic representation of the compounds investigated.

Results

Synthesis of mixed-metal [2×2] grid-type complexes: To avoid scrambling of the metal centers, it is necessary to first introduce the ruthenium(II) and osmium(II) ions. Complexes **Ru_2Fe_2** and **Os_2Fe_2**, each containing two different pairs of octahedral metal ions located at opposite corners, were obtained by reaction of the corresponding Ru^{II} or Os^{II} "corner" precursor **1-Ru** or **1-Os**, respectively, with Fe^{II} ions. Different strategies were employed to obtain **1-Ru** and **1-Os** from **1** (Scheme 2), while synthesis of the symmetric iron(II) grid was accomplished by using published protocols.[5,9]

In the case of **1-Ru**, it was necessary to proceed through the protection of one of the two binding sites by monomethylation of **1** by using trimethyoxonium tetrafluoroborate. Although **1** possesses six basic nitrogen sites, methylation of the terminal pyridine heterocycles was expected to be favored, since reaction at the central pyridine is subject to steric hindrance, and the pyrimidine nitrogen atoms are less nucleophillic. The reaction of **2b** with $RuCl_3$ in ethanol/water afforded the monoruthenium complex **3** in 48% isolated yield after purification by column chromatography.

 © 2003 Wiley-VCH Verlag GmbH & Co. KGaA, Weinheim

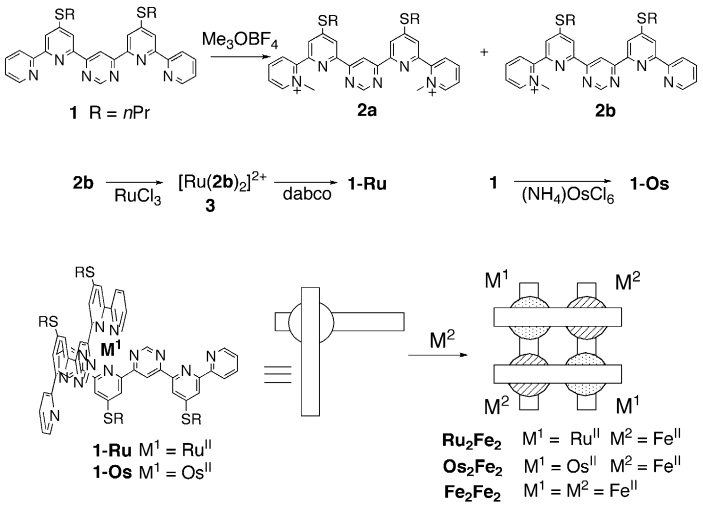

Scheme 2. Synthetic strategies for the assembly of the [2×2] grid-type complexes (bottom right) via the corner-type precursors (bottom left).

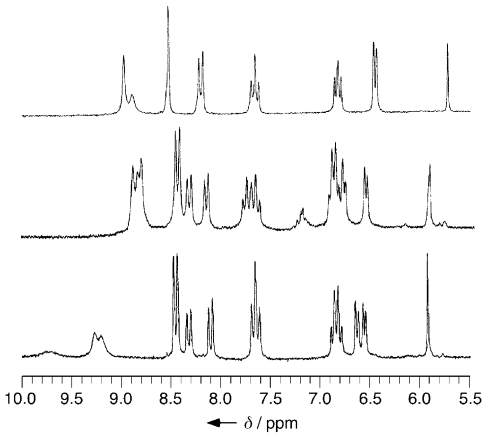

Figure 2. Aromatic portion of the ^{1}H NMR spectrum of the [2×2] grids: **Fe_2Fe_2**, (top), **Ru_2Fe_2** (middle), and **Os_2Fe_2** (bottom) containing a bound Cl^- ion that broadens the signals of the protons in the interior cavity.

Deprotection of the two vacant binding sites was achieved by demethylation with excess 1,4-diazabicyclo[2.2.2]octane (dabco) in refluxing acetonitrile to afford **1-Ru** as a dark purple solid in 66% yield after purification by chromatography. The compounds were characterized by FAB-mass spectrometry and ^{1}H NMR spectroscopy.

The necessity of the protection/deprotection approach is apparently a consequence of cooperativity in metal complexation by ligands containing bridging heterocyclic units. In the case of **1**, this may be due to increased electron density in the central pyrimidine ring resulting from complexation of the first metal ion, thus rendering coordination of the second ion more favorable. In contrast, the reaction of ammonium hexachloroosmate with two equivalents of **1** in refluxing ethylene glycol (5 h) proceeded smoothly to directly afford **1-Os** in 40% yield after purification by chromatography. Compared to Ru^{II}, the higher kinetic inertness of Os^{II} complexes may sufficiently slow down the reaction after complexation of one metal ion.

Addition of $Fe[BF_4]_2$ in acetonitrile to a solution of **1-Ru** or **1-Os** results in a gradual color change from deep purple to dark green over a period of a few minutes. Isolation and purification of the complexes formed yielded **Ru_2Fe_2** and **Os_2Fe_2** as dark green solids in 90% and 70% yield, respectively, after purification. The composition of the complexes was verified by MS(FAB), whereas the diagonal arrangement of the metal ions was confirmed by ^{1}H NMR spectroscopy (Figure 2), which showed different environments for the two binding sites of **1** in the complexes. During the purification, it was noted that the complexes have affinity for chloride ions, and the complete exchange of chloride by hexafluorophosphate counteranions required repeated precipitation from excess NH_4PF_6 solution. In the case of **Ru_2Fe_2**, MS(FAB) analysis of the complex resulting from incomplete anion exchange revealed the presence of at least one chloride ion, which was not lost during sample ionization. The presence of chloride ions also affected the ^{1}H NMR spectrum, particularly H2 and H5 of the central pyrimidine ring, which were considerably broadened and shifted downfield. Similar behavior was observed for **Os_2Fe_2**. The investigations of the spectroscopic and redox properties were conducted on the complexes from which the chloride ions were completely exchanged. Strong binding of chloride to a pentanuclear circular helicate has been reported by one of our groups.[10]

Solid-state structure of the Ru_2Fe_2 grid complex: The crystal structure of **Ru_2Fe_2** has been determined.[9] It confirmed the [2×2] grid structure of the complex, with like metal ions located at opposite corners of the assembly. Both the Ru and Fe ions are in a distorted octahedral environment, in which the terminal pyridine rings are pulled in towards the metal center. Whereas [2×2] grid structures with four identical metal ions are achiral, **Ru_2Fe_2** is chiral and both enantiomers are present in the unit cell. The packing within the crystal induces the grids to be aligned along the *b* axis of the crystal lattice, thereby placing the plane formed by the four metal ions in the *ab* plane of the lattice. This is of interest as it leads to a highly ordered solid-state structure in which each enantiomer is organized in a single plane (the *ac* plane).

Spectroscopic, luminescence, and redox properties: All the compounds exhibit very intense absorption bands in the UV region (ε in the 10^5–$10^6\,M^{-1}\,cm^{-1}$ range) as well as intense bands (ε in the 10^4–$10^5\,M^{-1}\,cm^{-1}$ range) that extend to the entire visible region (with the exception of **1-Ru** for which the absorption at wavelengths longer than 650 nm is negligible). Figure 3 shows the absorption spectra of all the compounds in acetonitrile. The mononuclear species **1-Ru** and **1-Os** exhibit relatively intense luminescence, both in acetonitrile at room temperature and in butyronitrile rigid matrices at 77 K. In all the cases, the luminescence decays are strictly monoexponential; lifetimes are in the 10^{-8}–10^{-7} s range at room temperature and approximately one or two orders of magnitude longer at 77 K. In contrast, the tetranuclear molecular grids do not exhibit any luminescence signals, even in the near IR region (up to 1000 nm), both at room temperature and at 77 K. The luminescence spectra of both the mononuclear complexes are shown in Figure 4, and

© 2003 Wiley-VCH Verlag GmbH & Co. KGaA, Weinheim

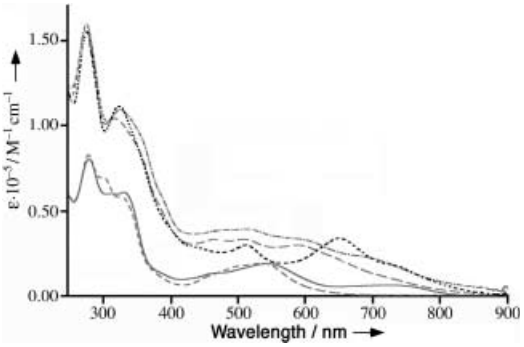

Figure 3. Absorption spectra of **1-Ru** (– – –), **1-Os** (——), Fe_2Fe_2 (-----), Ru_2Fe_2 (– – –), and Os_2Fe_2 (–·–·) in acetonitrile.

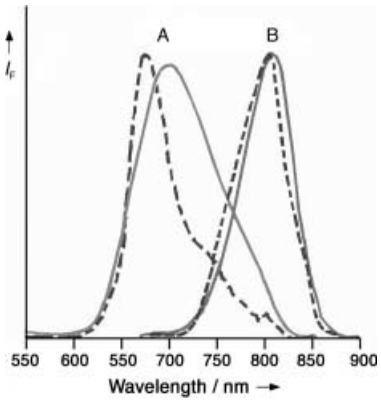

Figure 4. Normalized luminescence spectra (arbitrary units) of **1-Ru** (A spectra) and **1-Os** (B spectra) in acetonitrile at 298 K (solid lines) and in butyronitrile rigid matrix at 77 K (dashed lines). Spectra are uncorrected for detector response. Corrected maxima values are given in Table 1.

their absorption and luminescence data are collected in Table 1.

All the compounds undergo several redox processes, most of them reversible, in the potential window investigated (+2.00/−2.00 V vs SCE). Some of the oxidation processes are bielectronic in nature. The redox potentials are gathered in Table 2. The cyclic voltammograms obtained for Fe_2Fe_2, Ru_2Fe_2, and Os_2Fe_2 are shown in Figures 5–7.

Table 1. Spectroscopic and photophysical data of the mononuclear complexes studied. Data are in deoxygenated acetonitrile solution at 298 K, unless otherwise stated.

Compound	Absorption	Luminescence				
		298 K			77 K [a]	
	λ_{max} [nm] (ε [$M^{-1}cm^{-1}$])	λ_{max} [nm]	τ [ns]	Φ	λ_{max} [nm]	τ
1-Ru	279 (80420)	720	59	2.45×10^{-3}	685	4.95 μs
	302 (67300)					
	329 (56350)					
	454 (10620)					
	500 (16640)					
	543 (18190)					
1-Os	279 (77820)	825	18	1.83×10^{-3}	820	630 ns
	331 (58980)					
	462 (12540)					
	549 (19570)					
	762 (5840)					

[a] In butyronitrile rigid matrix at 77 K.

Table 2. Redox data in acetonitrile solution. In the case of multielectron processes, the number of exchanged electrons is reported in square brackets.

	$E_{1/2}$ (ox) [V vs SCE]	$E_{1/2s}$ (red) [V vs SCE]
1-Ru	+1.31	−0.85; −1.02; −1.52; −1.60[a]
1-Os	+0.96	−0.81; −1.03; −1.54; −1.82[a]
Fe_2Fe_2	+1.35; +1.40; +1.59; +1.76	−0.25; −0.32; −0.46; −0.52; −1.09; −1.19; −1.38; −1.46
Ru_2Fe_2	+1.32; +1.38; +1.67	−0.27; −0.32; −0.46; −0.51; −1.07; −1.17; −1.35[a]
Os_2Fe_2	+1.15 [2]; +1.53 [2]	−0.30 [2]; −0.51; −0.57; −1.04; −1.15

[a] Adsorption on the electrode.

Discussion

The metallosupramolecular grid species studied herein are based on metal polypyridine-type complexes, and their spectroscopic, photophysical, and redox properties can be discussed within the framework of a localized molecular orbital approximation.[11] Within this approximation, the electronic transitions and excited states can be classified as metal centered (MC), ligand centered (LC), and charge transfer (either metal-to-ligand, MLCT, or ligand-to-metal, LMCT), while the redox processes can be considered as either metal or ligand centered.

Electronic absorption spectra: On the basis of the known absorption properties of polypyridine metal complexes,[11] the intense absorption features in the UV region exhibited by all the compounds investigated here (Table 1, Figure 3) are assigned to spin-allowed LC electronic transitions involving the polypyridine ligands. The electronic transitions in the visible region up to 620 nm (Table 1, Figure 3) can be attributed to spin-allowed MLCT transitions. This assignment is supported by the observation that the band at approximately 535 nm in **1-Ru** is similar to the MLCT band of a closely related complex, $[Ru(\mathbf{4})(terpy)]^{2+}$ (**4** = 2-(9-anthryl)-4,6-bis(2′,2″-bipyridyl-6′-yl)pyrimidine; terpy = 2,2′:6′,2″-terpyridine), for which the lowest-lying spin-allowed MLCT band (namely, the Ru→**4** CT band) exhibits a maximum at 510 nm.[12] The moderately intense band at $\lambda >$ 620 nm that is present in **1-Os** is assigned to spin-forbidden MLCT transitions.[13] In the tetranuclear grid Ru_2Fe_2, the MLCT band is expected to move towards the red with respect to the mononuclear species as a consequence of the stabilization of the ligand-centered orbitals upon double metal coordination, as often found for bis-chelating polypyridine ligands with interacting chelating sites.[14] Comparison of the absorption spectra of Ru_2Fe_2 (Figure 3) with those of the rack-type [(terpy)Ru(μ-**4**)-

 © 2003 Wiley-VCH Verlag GmbH & Co. KGaA, Weinheim

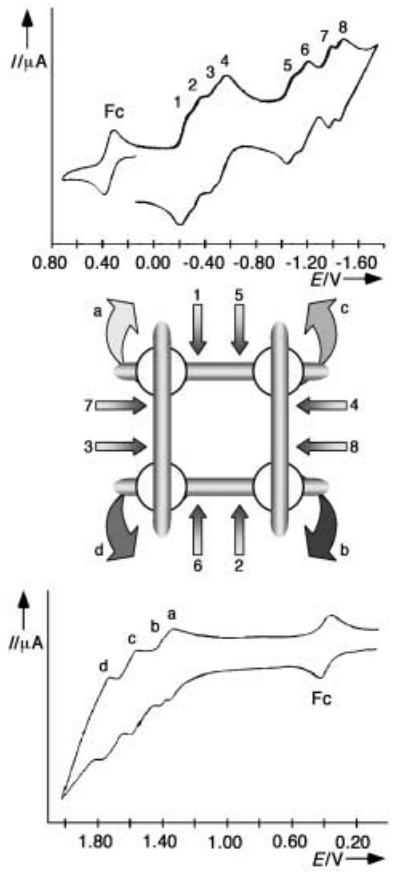

Figure 5. Electrochemical redox properties of the Fe_2Fe_2 grid. Cyclic voltammetry curves in acetonitrile. Top: reduction; bottom: oxidation. Potentials are given versus SCE. In the middle, assignment of the various oxidation (a–d) and reduction (1–8) processes to specific sites is schematized (see text for details). Fc stands for ferrocene, used as an internal reference.

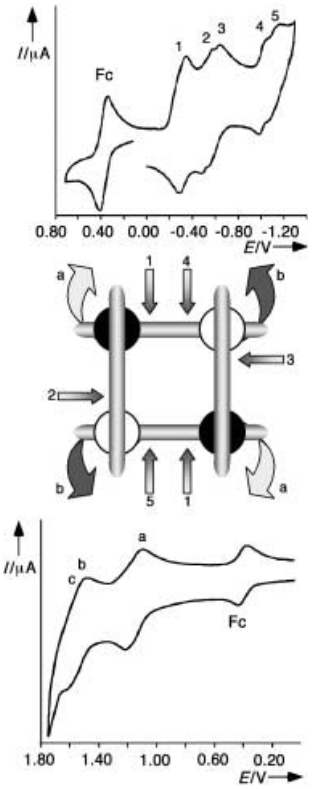

Figure 6. Electrochemical properties of the Os_2Fe_2 grid. Cyclic voltammetry curves in acetonitrile. Top: reduction; bottom: oxidation. Potentials are given versus SCE. In the middle, assignment of the various oxidation (a–d) and reduction (1–5) processes to specific sites is schematized (see text for details). Fc stands for ferrocene, used as an internal reference.

$Ru(terpy)]^{4+}$ and related complexes[15] allows us to assign the broad band around 600 nm of $\mathbf{Ru_2Fe_2}$ to Ru→**1** CT transitions. By comparing the spectra of the three molecular grids (Figure 4), it is possible to assign the bands at 610 nm in $\mathbf{Os_2Fe_2}$ and at 660 nm in $\mathbf{Fe_2Fe_2}$ to spin-allowed Os→**1** CT and Fe→**1** CT transitions, respectively. Moreover, the band in the 650–800 nm region of $\mathbf{Os_2Fe_2}$ is likely to be a spin-forbidden MLCT transition, benefiting from mixing with the spin-allowed transitions because of the stronger spin-orbit coupling induced by the heavy osmium center.[16] In all the grids, the presence of Fe^{II}-containing subunits suggests the existence of low-energy MC transitions. However, such transitions are symmetry-forbidden and are probably obscured by the more intense MLCT bands.

Luminescence properties: The luminescence of **1-Ru** and **1-Os** (Figure 4, Table 1), both at room temperature and at 77 K, is assigned to ^{3}MLCT excited states. This is based on the emission energies, lifetimes, and quantum yields of the complexes, which are in good agreement with literature data for similar species.[11] In this respect, the room temperature luminescence of **1-Ru** is comparable to $[Ru(\mathbf{4})terpy)]^{2+}$ ($\lambda_{max}=715$ nm; $\tau=30$ ns; $\Phi=1.5\times10^{-3}$),[12] further confirming the ^{3}MLCT origin of the emission. The room-temperature emission spectrum of **1-Os** is red-shifted compared to that of **1-Ru**, in agreement with the known differences in the MLCT states of analogous Ru^{II} and Os^{II} complexes, which is directly related to the difference in oxidation behavior of the two metal centers.

The room-temperature luminescence of **1-Ru** is not a straightforward result. In fact, Ru^{II} complexes that contain tridentate polypyridine ligands are rarely luminescent at room temperature (and in case they are, their luminescence quantum yields are usually weak and short-lived,[15,17] with few exceptions[11,18]). The reason lies in the geometrical distortion of the octahedral metal coordination imposed by tridentate chelates. Such a distortion reduces the ligand field strength experienced by the metal and, therefore, the energy gap between the (fully occupied, in a d^6 configuration) t_{2g} and the (empty) e_g metal-centered orbitals. Therefore, in Ru^{II} complexes with tridentate ligands, MC levels are lower in energy than in similar complexes that contain bidentate ligands and lie very close to the potentially emitting MLCT levels. The consequence is that such low-lying MC levels strongly contribute to deactivate through radiationless pathways the MLCT states by thermally activated surface-crossing processes.[11,16] This problem appears to be alleviated in **1-Ru**, probably by the stabilization of the luminescent MLCT level, which reduces the effect of the thermally activated process.

© 2003 Wiley-VCH Verlag GmbH & Co. KGaA, Weinheim

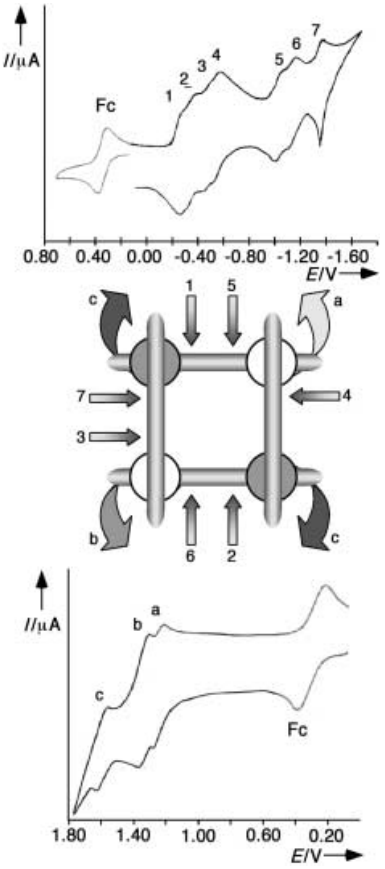

Figure 7. Electrochemical redox properties of the $\mathbf{Ru_2Fe_2}$ grid. Cyclic voltammetry curves in acetonitrile. Top: reduction; bottom: oxidation. Potentials are given versus SCE. In the middle, assignment of the various oxidation (a–d) and reduction (1–7) processes to specific sites is schematized (see text for details). Fc stands for ferrocene, used as an internal reference.

Metal-centered excited states in Os^{II} complexes lie at much higher energy than in Ru^{II} complexes, so that emission from **1-Os** was expected. However, the similarity of room temperature and 77 K emission spectra for this species, in particular the small difference in emission energy (Table 1, Figure 4) warrants some discussion. Generally, Ru^{II} and Os^{II} polypyridine luminescence spectra are significantly blue-shifted on passing from room temperature fluid solution to 77 K rigid matrix[11,14,19] due to their charge-transfer character.[20] The origin of the blue-shift is mainly due to the solvent reorganization occurring in the CT excited states. In fluid solution, this process is normally much faster than the decay processes to the ground state and stabilizes the CT states before emission takes place (so decreasing the emission energy). However, the solvent reorganization processes are hampered in rigid matrices and cannot stabilize the luminescent levels. The difference in energy between fluid solution and rigid matrix emission spectra in CT emitters can therefore be used to infer information on the extent of the charge-transfer process inherent to the MLCT excitation. The larger the energy difference between emission in fluid solution and in rigid matrices, the larger is the extent of the charge-transfer character of the excited state responsible for the emission. From the data presented in Table 1 and Figure 4, it appears that the emission spectrum of **1-Os** undergoes an almost negligible shift on going from fluid solution to a frozen matrix, suggesting that the charge-transfer character of the (formally) ^{3}MLCT state is rather small. This may be due to strong Os-to-ligand π-backbonding in the ground state, a consequence of the relatively easy-to-oxidize Os^{II} center and the easy-to-reduce ligand **1** (see redox data). A non-negligible partial metal-to-ligand charge-transfer character would therefore already be present in the ground state, making it quite similar to the MLCT state as far as the electronic distribution is concerned.

The lowest lying excited states of Fe^{II} polypyridine complexes are highly distorted MC states that deactivate by fast radiationless decay to the ground state, and these complexes are usually not luminescent.[16b] Whereas the absence of emission of $\mathbf{Fe_2Fe_2}$ is therefore expected, the absence of luminescence for the heteronuclear grids $\mathbf{Ru_2Fe_2}$ and $\mathbf{Os_2Fe_2}$ is not evident. Good models for the excited state of the Ru^{II}-based subunits contained in $\mathbf{Ru_2Fe_2}$ are the previously investigated rack-type $[(terpy)Ru(\mathbf{4})Ru(terpy)]^{4+}$ and $[(terpy)Ru(\mathbf{5})Ru(terpy)]^{4+}$ complexes (**5** = 4,6-bis(2′,2″-bipyridyl-6′-yl)pyrimidine).[15] The excited state properties of both these latter complexes are governed by triplet Ru→**4** and Ru→**5** CT states, respectively, which should be very similar to the lowest-energy levels of the Ru^{II}-based components of $\mathbf{Ru_2Fe_2}$. The rack-type species mentioned above exhibit luminescence at around 850 nm in acetonitrile and at around 780 nm in rigid matrix at 77 K.[15] By comparison, $\mathbf{Ru_2Fe_2}$ should exhibit similar emission properties if the Ru^{II}-based chromophores are isolated from the other components of the grid structure. Although literature data for compounds containing Os^{II}-based subunits similar to those that are present in the $\mathbf{Os_2Fe_2}$ molecular grid are lacking, it can be foreseen that emission from these subunits should occur at wavelengths shorter than 1000 nm, on the basis of comparison between the photophysical properties of homologous Ru^{II} and Os^{II} polypyridine complexes.[14] However, even by employing a near-infrared sensitive luminescence spectrometer, we were unable to detect emission for the mixed-metal grid $\mathbf{Os_2Fe_2}$. These results clearly indicate that an intra-assembly pathway leading to the ultrafast deactivation of the Ru- and Os-based excited states is present in both of the mixed-metal grids. Most likely, the deactivation mechanism involves fast energy transfer from the ^{3}MLCT states of the Ru^{II} or Os^{II} centers to the ^{3}MC levels of the Fe^{II}-based subunits.

Recent investigations, with pump-probe femtosecond spectroscopy, have shown that the rate constants of photoinduced energy transfer between Ru- and Os-based subunits in multinuclear complexes based on the 2,3-bis(2′-pyridyl)-pyrazine bridging ligand (which is similar to the bridging ligand **1** used here as far as the electronic interactions allowed between the metal centers are concerned) exceed 5×10^{12} s^{-1}.[21] Since rate constants of similar order of magnitude for the intercomponent energy-transfer processes occurring in the molecular grids here investigated can be inferred, quenching of the Ru- and Os-based luminescence by energy transfer to Fe-based excited states is perfectly justified.[22] Therefore, in the mixed-metal grids the electronic energy

 © 2003 Wiley-VCH Verlag GmbH & Co. KGaA, Weinheim

collected by light absorption by all of the subunits appears to be efficiently channeled to the component(s) where the lowest-energy excited states are located (in the present case, the Fe^{II} subunits).

Redox behavior

Oxidation processes: For all the complexes investigated, the reversibility (or in some cases, the quasi-reversibility) of the processes suggests that all the oxidations are metal centered.[11] Therefore, the assignment of the oxidation processes of **1-Ru** and **1-Os** (Table 2) is straightforward. Furthermore, their half-wave potentials are in good agreement with those of other Ru^{II} and Os^{II} polypyridine complexes.[11,14,16] The assignment of the oxidation processes of the three molecular grids to specific sites of the multicomponent structures is more complicated, since each species contains four redox-active metal centers. For the sake of simplicity, we start our discussion with the homonuclear grid $\mathbf{Fe_2Fe_2}$ (Table 2, Figure 5 bottom). This species undergoes four mono-electronic reversible oxidation processes. Following the first oxidation of one of the four identical metal centers, a second oxidation process is observed at a potential only slighly more positive than the first ($\Delta E_{1/2} = 50$ mV). Because redox data of dinuclear Ru^{II} complexes containing a bridging pyrimidine ring ($\Delta E_{1/2} = 300$ mV for [(terpy)Ru(**4**)Ru(terpy)]$^{4+}$[23]) indicate that there is significant electronic interaction between metal centers connected to the same bridge in these type of complexes, it can be concluded that the second oxidation process involves the Fe^{II} center which is farthest away, that is, diagonal to the first oxidized center (Figure 5, middle). The third oxidation process concerns one of the two other Fe^{II} centers. Its potential is significantly more positive than the second one ($\Delta E_{1/2} = 190$ mV), in agreement with the presence of two nearby (formally) Fe^{III} centers. The fourth oxidation involves of course the remaining Fe^{II} center.

It is interesting to note that the separation of the third and fourth oxidation processes (170 mV), which depends on the electronic interactions between two opposite corners of the molecular grids when the other corners are Fe^{III} centers, is larger than the separation between the first two processes (50 mV), in turn depending on the electronic interactions between two opposite corners of the molecular grids when the other corners are Fe^{II} centers. Such a difference clearly indicates that the electronic interaction between two redox-active sites localized at opposite corners of $\mathbf{Fe_2Fe_2}$ is a function of the oxidation state of the other redox-active sites.The $\mathbf{Os_2Fe_2}$ grid exhibits two reversible oxidation processes, both of them bi-electronic in nature (Table 2, Figure 6 bottom). The assignment of these processes is based on the oxidation data of the mononuclear **1-Os** complex and of the homonuclear grid $\mathbf{Fe_2Fe_2}$. The half-wave potential value of the first wave indicates that it can be assigned to the simultaneous one-electron oxidation of both the Os^{II} centers (it should be recalled that metal coordination of the second binding site of a bridging ligand stabilizes the orbitals of the first metal, so shifting the first oxidation process of the multinuclear species to more positive values compared to the mononuclear precursor[14,24]). The second process can therefore be assigned to the simultaneous one-electron oxidation of two Fe^{II} centers. The potential value of this latter oxidation process is in good agreement with that of the third oxidation of $\mathbf{Fe_2Fe_2}$, confirming the attribution. On the basis of the redox data of $\mathbf{Fe_2Fe_2}$, the bi-electronic nature of the oxidation processes of $\mathbf{Os_2Fe_2}$, which suggests that the electronic interactions between opposite corners is negligible from an electrochemical viewpoint for this latter species, is somewhat puzzling. Apparently, the presence in $\mathbf{Os_2Fe_2}$ of two pairs of metal centers with substantially different electronic properties from one another (as indicated by the comparison between the oxidation potential of the mononuclear Os^{II} complex **1-Os** and the first oxidation potential of $\mathbf{Fe_2Fe_2}$) has the effect of "isolating" the redox-active sites. We have no simple explanation for such a behavior at the moment.

The assignment of the oxidation processes of $\mathbf{Ru_2Fe_2}$ (Table 2, Figure 7, bottom) is more complicated. A good model for the first oxidation potential of Ru^{II}-based centers is the first oxidation process of the rack-type complex [(terpy)Ru(**4**)Ru(terpy)]$^{4+}$, which occurs at $+1.45$ V.[23] Since the potentials of the first and second oxidation processes of $\mathbf{Ru_2Fe_2}$ ($+1.32$ V and $+1.38$ V) are quite similar to those of the first and second oxidation process of $\mathbf{Fe_2Fe_2}$ ($+1.35$ V and $+1.40$ V), and are in both cases less positive than that of the first Ru^{II} oxidation process in the model mentioned above, we assign the first two oxidation processes of $\mathbf{Ru_2Fe_2}$ to successive oxidation of the two Fe^{II} centers. In agreement with such an assignment, the separation between the two processes (60 mV) is comparable to the separation of the first two oxidation processes in $\mathbf{Fe_2Fe_2}$ (see above). The subsequent oxidation process is not fully reversible, so it cannot be stated if it involves one or two electrons. Anyway, it can be attributed to the Ru^{II} centers.

Reduction processes: The assignment of the reduction processes of **1-Ru** and **1-Os** (Table 2) is straightforward. For each complex, the first two reduction processes are assigned to the first one-electron reduction of each ligand, and the third process can be attributed to the second reduction of one of the ligands. The fourth reduction occurs at more negative potentials, but its potential cannot be determined precisely because of adsorption of the complex on the electrode. The separation between the second and third reduction processes (about 500 mV), correlates with the pairing energy in the lowest π^* orbital of **1**, which is in agreement with the values for the pairing energy of similar polypyridine ligands.[6,25]

On passing to the grid complexes, we have to recall that the reductions of bridging ligands in polynuclear complexes are usually shifted to less negative potentials relative to the reductions of the same ligands in mononuclear complexes; this is a consequence of the stabilization in bridging ligand orbitals induced by the additional metal(s). For $\mathbf{Fe_2Fe_2}$ (Table 2, Figure 5 top), the first reduction most likely involves a ligand orbital that has a large contribution from the pyrimidine ring, which, beside having its LUMO lower than those of the pyridine rings, is also coordinated by two metal centers. The second reduction takes place at a potential that is more negative by 70 mV. Because the interaction between

© 2003 Wiley-VCH Verlag GmbH & Co. KGaA, Weinheim

two identical ligands coordinated to the same metal center in these complexes can be inferred by the separation between the two first reduction processes of the mononuclear species (about 200 mV), the relatively small difference in potential between the first two reduction processes of $\mathbf{Fe_2Fe_2}$ indicates that the second reduction involves the bridging ligand which is opposite to the first one (Figure 5 middle). On the basis of the above discussion, the third and fourth processes are assigned to one-electron reduction of the other two bridging ligands. The separation between the second and third processes (140 mV) and third and fourth ones (60 mV) supports the assignment and points out the dependence of the electronic interaction between ligands on their relative location. At potentials more negative than −1.00 V, $\mathbf{Fe_2Fe_2}$ exhibits four additional, quasi-reversible, processes. These are assigned to the second one-electron reduction of each ligand, following the same sequence of the first four processes. The pairing energy in the bridging ligand, related to the separation between the fourth and fifth processes (540 mV), is comparable to that found for the mononuclear species.

The reduction properties of $\mathbf{Fe_2Fe_2}$ are in good agreement with those recently reported for other homometallic [2×2] grids based on Co^{II}, Zn^{II}, and Mn^{II}, as well as on Fe^{II} grids containing slightly different bridging ligands.[6] As far as the heterometallic grids are concerned, it can be noted that the reduction pattern of $\mathbf{Ru_2Fe_2}$ (Table 2, Figure 6 top) is very similar to that of $\mathbf{Fe_2Fe_2}$, with the exception that the seventh process coincides with adsorption at the electrode. The assignment of the observable reduction processes of this species is therefore identical to the corresponding processes of $\mathbf{Fe_2Fe_2}$. In contrast, the reduction pattern of $\mathbf{Os_2Fe_2}$ (Table 2, Figure 7 top) is different from that of the other two grids, as well as from that of other homometallic [2×2] grids.[6] In fact, the first process is bi-electronic in nature and can be assigned to two one-electron reductions, involving two identical and non-interacting sites. By comparison with the other systems presented here, these are identified as two bridging ligands facing one another. This suggests that in $\mathbf{Os_2Fe_2}$ the interaction between these ligands is negligible. Here also, the reason of such a behavior may lie in the electronic differences between Os^{II} and Fe^{II}, which are much larger than the differences between Ru^{II} and Fe^{II}. This effectively makes each bridging ligand more "dissymmetric" with respect to the central pyrimidine from an electronic viewpoint and might explain the coalescence of the two first reduction waves.[26] The two subsequent reduction processes are attributed to successive one-electron reductions of the remaining two bridging ligands, while the remaining processes are analogous to those of the other grids. The important role of the metal ion in isolating (e.g., Zn^{II}) or conversely, in providing communication (e.g., Co^{II}) between the ligands in [2×2] grid complexes has been discussed earlier.[6]

Conclusion

The metallosupramolecular [2×2] grid type species and their mononuclear precursors investigated here exhibit quite interesting spectroscopic and redox properties. Their absorption spectra are dominated by LC and MLCT bands, most of which can be assigned to specific components of the supramolecular structures. While the mononuclear Ru^{II} and Os^{II} precursors exhibit relatively intense ^{3}MLCT luminescence, the (potentially luminescent) Ru^{II}- and Os^{II}-based ^{3}MLCT excited states in the heteronuclear grids are quantitatively quenched, most likely by intercomponent energy transfer to the (nonluminescent) lower lying ^{3}MC states of the Fe^{II} subunits. This result suggests that the multicomponent molecular grids investigated here can behave as efficient light-harvesting antennas, because all the light absorbed by the various subunits is efficiently channelled to the subunit(s) in which the lowest-energy excited states are located.

All the species exhibit a very rich redox behavior, and all the redox processes can be assigned to specific components; in particular, for $\mathbf{Fe_2Fe_2}$ it has been possible to identify up to twelve different redox states. Therefore, these systems can be viewed as multilevel molecular electronic species,[6] capable of exchanging a number of electrons at accessible and predetermined potentials in a reversible way. Furthermore, it has also been found that the electronic interaction between specific subunits depends on their location in the structure as well as on the nature and the oxidation states of the other components, in line with the redox properties of Zn^{II} and Co^{II} [2×2] grids studied earlier.[6] This last result suggests that, in principle, it is possible to tune the extent of the electronic interactions between specific subunits by the use of suitable inputs, for example, external potentials. Such a behavior is of particular significance with respect to information storage through localized electron exchange amounting to "bit" generation in well-defined patterns.[1b] Grid-type structures may thus present much potential as functional supramolecular devices for information storage and processing.

Experimental Section

Materials and methods: ^{1}H and ^{13}C NMR spectra were recorded on a Bruker AC200 instrument at 200 and 50 MHz, respectively, with the residual solvent peak as reference. THF was dried over Na/benzophenone and distilled prior to use. DMF and DMSO were dried over molecular sieves. Other reagents were used as received without further purification. Chromatography was carried out on Merk 60 silica gel (0.040–0.200 mm), or Merk activity II–III alumina (0.063–0.200 mm). The synthesis of 4,6-bis[4-(*n*-thiopropyl)-6-(pyrid-2-yl)pyrid-2-yl]pyrimidine (**1**) has been described previously.[27]

Electronic absorption spectra were recorded on a Hitachi U-3300 spectrophotometer. For steady-state luminescence measurements at wavelengths shorter than 900 nm, a Jobin Yvon-Spex Fluoromax 2 spectrofluorimeter was used, equipped with a Hamamatsu R3896 photomultiplier, and the spectra were corrected for photomultiplier response using a program purchased with the fluorimeter. For detecting (eventual) luminescence at wavelength longer than 900 nm, the 514 nm line of a Spectra-Physics 265 Ar laser was used for excitation in a modified Edinburgh FS900 spectrofluorimeter. Detection was accomplished by using a cooled (77 K) North Coast EO-817 L Ge detector in combination with a Stanford Research SR lock-in amplifier. For the luminescence lifetimes, an Edinburgh FL 900 single-photon-counting spectrometer was used (nitrogen discharge; pulse width, 3 ns).

 © 2003 Wiley-VCH Verlag GmbH & Co. KGaA, Weinheim

Emission quantum yields were measured at room temperature by using the optically dilute method.[28] $[Os(bpy)_3]^{2+}$ in deaerated acetonitrile was used as a quantum yield standard, assuming a value of 0.0066.[29]

Electrochemical measurements were carried out in argon-purged acetonitrile at room temperature with PAR 273 multipurpose equipment interfaced to a PC. The working electrode was a glassy carbon (8 mm^2, Amel) electrode. The counter electrode was a Pt wire, and the reference electrode was an SCE separated with a fine glass frit. The concentration of the complexes was about 5×10^{-4} M. Tetrabutylammonium hexafluorophosphate was used as supporting electrolyte and its concentration was 0.05 M. Cyclic voltammograms were obtained at scan rates of 20, 50, 200, and 500 $mV\,s^{-1}$. For reversible processes, half-wave potentials (vs SCE) were calculated as the average of the cathodic and anodic peaks. The criteria for reversibility were the separation of 60 mV between cathodic and anodic peaks, the close to unity ratio of the intensities of the cathodic and anodic currents, and the constancy of the peak potential on changing scan rate. The number of exchanged electrons was measured with differential pulse voltammetry (DPV) experiments performed with a scan rate of 20 $mV\,s^{-1}$, a pulse height of 75 mV, and a duration of 40 ms, and by taking advantage of the presence of ferrocene used as the internal reference.

Experimental uncertainties are as follows: absorption maxima, ±2 nm; molar absorption coefficient, 10%; emission maxima, ±5 nm; excited state lifetimes, 10%; luminescence quantum yields, 20%; redox potentials, ±10 mV.

Synthesis

Compounds 2a and 2b: Trimethyloxonium tetrafluoroborate (0.50 g, 3.58 mmol) was placed in a dry 50 mL round-bottomed flask and ground to a fine powder with a glass rod under an argon atmosphere. After addition of **1** (1.40 g, 2.55 mmol), the flask was fitted with a condenser topped with a septum and the entire apparatus flushed with argon. Thirty milliliters of 1,2-dichloroethane (previously dried over CaH_2) was added through a cannula, and the mixture was refluxed 4 h. Et_3N (1 mL) was then added to the cooled mixture, and the solvents removed on a rotary evaporator. The solid was boiled in acetonitrile (20 mL) and filtered to recover unreacted **1** (0.50 g, 36%) as a fluffy solid. The acetonitrile was removed and the solid taken up in hot ethanol, cooled, and filtered to give 1.28 g of a mixture of **2a** and **2b** as a white solid (the yellow filtrate contains principally triethylamine salts). Separation was easily achieved by column chromatography (alumina, 2:1 acetonitrile/toluene, R_f(**2a**)= 0.22, R_f(**2b**)=0.76) to yield 0.61 g (37%) of **2b** and 0.46 g (24%) of **2a**. Compound **2a**: MS (FAB+): *m/z* (%): 780.1 (100) [M^+]; compound **2b** ^{1}H NMR: δ=1.10 (t, J=8 Hz, 3H), 1.13 (t, J=8 Hz, 3H), 1.70–1.92 (m, 4H), 3.12 (t, J=8 Hz, 3H), 3.21 (t, J=8 Hz, 3H), 7.48 (br dd, 1H), 7.72 (s, 1H), 7.95 (t, J=6 Hz, 1H), 8.12 (t, J=6 Hz, 1H), 8.29 (t, J=6 Hz, 1 Hz), 8.29 (s, 1H), 8.32 (s, 1H), 8.49 (d, J=6 Hz, 1H), 8.62 (s, 1H), 8.64 (d, J=6 Hz, 1H), 8.69 (d, J=6 Hz, 1H), 8.85 (d, J=6 Hz, 1H), 9.24 (s, 1H), 9.30 (s, 1H).

Complex $[Ru(2b)_2][PF_6]_4$ ($3[PF_6]_4$): A mixture of **2b** (0.811 g, 1.24 mmol) and ruthenium trichloride (0.162 g, 0.62 mmol) in EtOH/H_2O (1:1, 20 mL) was refluxed under argon for 16 h. The cooled black solution was poured in an aqueous NH_4PF_6 solution and the precipitate collected by filtration and washed well with water and air dried. The solid was recovered by dissolution with acetone and the product purified by column chromatography (silica, MeOH/NH_4Cl (2 M)/$MeNO_2$ 7:2:1). The red band was collected and the product recovered by addition of NH_4PF_6 followed by removal of the volatile organic solvents under reduced pressure and filtration. In cases where the material did not elute from the column, 10% v/v of aqueous ammonia was added to the eluent mixture. After drying under vacuum, 0.530 g (48%) of $\mathbf{3}[PF_6]_4$ were recovered as a red powder. ^{1}H NMR: δ=1.03 (t, J=8 Hz, 6H), 1.25 (t, J=8 Hz, 6H), 1.75 (sextuplet, J=8 Hz, 4H), 2.02 (sextuplet, J=8 Hz, 4H), 3.10 (t, J=8 Hz, 4H), 3.51 (t, J=8 Hz, 4H), 4.38 (s, 6H), 7.22 (br dd, 2H), 7.37 (d, J= 6 Hz, 2H), 7.71 (s, 2H), 7.98 (t, J=6 Hz, 2H), 8.21 (m, 6H), 8.29 (s, 2H), 8.59 (d, J=6 Hz, 2H), 8.63 (s, 2H), 8.70 (t, J=6 Hz, 2H), 8.84 (s, 2H), 8.91 (d, J=6 Hz, 2H), 9.22 (s, 2H); MS (FAB+): *m/z* (%): 1807 (0.5) [M^+], 1639 (5) [M^+-PF_6], 1494 (5) [M^+-2PF_6], 551 (100).

Complex $[Ru(1)_2][PF_6]_2$ (1-Ru): A solution of **3** (150 mg, 0.084 mmol) and dabco (750 mg, 6.70 mmol) were refluxed under argon in acetonitrile (12 mL) for 48 h. The solution was then poured into an aqueous NH_4PF_6 solution; the precipitate was collected by centrifugation, dissolved in acetone, and once again precipitated by addition to an aqueous NH_4PF_6 solution. Further purification was achieved by column chromatography (alumina, 2:1 acetonitrile/toluene). Evaporation of the purple band yielded 99 mg (80%) of **1-Ru** (·$2PF_6$). ^{1}H NMR: δ=0.70 (br t, 6H), 1.34 (t, J= 8 Hz, 6H), 1.34 (br m, 4H), 2.08 (sextuplet, J=8 Hz, 4H), 2.62 (br t, 4H), 3.51 (t, J=8 Hz, 4H), 7.18 (br dd, 2H), 7.33 (t, J=6 Hz, 2H), 7.57 (m, 6H), 8.01 (t, J=6 Hz, 2H), 8.13 (m, 4H), 8.34 (br s, 2H), 8.42 (br d, 2H), 8.63 (s, 2H), 8.68 (t, J=6 Hz, 2H), 8.75 (d, J=6 Hz, 2H), 8.82 (br s, 2H); MS (FAB+): *m/z* (%): 1381 (5) [M^+-PF_6], 1174 (8) [M^+-2PF_6], 629 (30).

Complex $[Os(1)_2][PF_6]_2$ (1-Os): A mixture of **1** (550 mg, 1.00 mmol) and ammonium hexachloroosmate (219 mg, 0.50 mmol) in ethylene glycol (20 mL) was purged with argon and plunged into an oil bath heated to 100 °C. The temperature was then increased to 220 °C and stirring continued for 5 h. The cooled solution was then poured into an aqueous NH_4PF_6 solution, and the black solid was collected by filtration and washed well with water. Purification by column chromatography (alumina, 2:1 acetonitrile/toluene, fast-moving purple band) yielded 305 mg (39%) of **1-Os** (·$2PF_6$) as a black powder. ^{1}H NMR: δ=0.89 (br t, 6H), 1.32 (t, J=8 Hz, 6H), 1.60 (br m, 4H), 2.0 (sextuplet, overlays with residual solvent, 4H), 2.94 (br t, 4H), 3.56 (t, J=8 Hz, 4H), 7.19 (br dd, 2H), 7.29 (br d, 2H), 7.53 (dd, J_1=6 Hz, J_2=4 Hz, 4H), 7.81 (br dd, 2H), 7.90 (s, 2H), 8.10 (s, 2H), 8.50 (dd, J_1=8 Hz, J_2=2 Hz, 4H), 8.61 (t, J=8 Hz, 2H), 8.68 (s, 2H), 8.81 (br s, 2H), 8.85 (br d, 2H), 9.24 (br s, 2H); MS (FAB+): *m/z* (%): 1554 (3) [M^+], 1409 (100) [M^+-PF_6], 1264 (100) [M^+-2PF_6].

Complex $[\{Ru(1)\}_2\{Fe(1)\}_2][PF_6]_8$ (Ru_2Fe_2): Precursor **1-Ru** (20.0 mg, 13.66 μmol) and iron(II)tetrafluoroborate hexahydrate (7.00 mg, 20 μmol) were placed in a 10 mL round-bottomed flask. Upon addition of acetonitrile, the solution rapidly turned dark green. Stirring was continued overnight, and the product precipitated by addition of TBAC and dilution with diethyl ether. The solid was collected and purified by column chromatography (silica, MeOH/NH_4Cl (2 M)/$MeNO_2$ 7:2:1). The green band was collected and the product recovered by addition of NH_4PF_6 followed by removal of the volatile organic solvents under reduced pressure and filtration. Reprecipitation with aqueous NH_4PF_6 solution and drying yielded 15.26 mg of $\mathbf{Ru_2Fe_2}\cdot7PF_6\cdot Cl$ (62%) as a dark green solid. Complete anion exchange requires repeated reprecipitation from aqueous NH_4PF_6 solution. ^{1}H NMR: δ=1.35 (t, J=8 Hz, 12H), 1.39 (t, J=8 Hz, 12H), 2.1 (m, overlaps with residual solvent, 16H), 3.70 (m, 16H), 5.97 (s, 4H), 6.59 (d, J=6 Hz, 4H), 6.80–6.95 (m, 12H), 7.68 (t, J=6 Hz, 4H), 7.77 (t, J=6 Hz, 4H), 8.19 (d, J=6 Hz, 4H), 8.35 (d, J=6 Hz, 4H), 8.43 (s, 4H), 8.47 (s, 4H), 8.80 (s, 4H), 8.83 (s, 4H), 8.89 (s, 4H); MS (FAB+) of $\mathbf{Ru_2Fe_2}\cdot7PF_6Cl$: *m/z* (%): 3365 (20) [$M^+-PF_6$], 3220 (55) [$M^+-2PF_6$], 3072 (2) [$M^+-3PF_6$]; elemental analysis calcd (%) for $C_{120}H_{112}F_{42}ClN_{24}P_7S_8Ru_2Fe_2$: C 41.05, H 3.21, N 9.57; found: C 40.94, H 3.32, N 9.47.

Complex $[\{Os(1)\}_2\{Fe(1)\}_2][PF_6]_8$ (Os_2Fe_2): Precursor **1-Os** (60.0 mg, 38.61 μmol) and iron(II)tetrafluoroborate hexahydrate (24.00 mg, 71.22 μmol) were placed In a 10 mL round-bottom flask. Upon addition of acetonitrile, the solution rapidly turned dark green. Stirring was continued at room temperature overnight, and the product precipitated by addition of TBAC and dilution with toluene. The solid was collected and purified by column chromatography (silica, MeOH/NH_4Cl (2 M)/$MeNO_2$ 7:2:1). The green band was collected and the product recovered by addition of NH_4PF_6 followed by removal of the volatile organic solvents under reduced pressure and filtration. Reprecipitation with aqueous NH_4PF_6 solution and drying yielded 49.7 mg of $\mathbf{Os_2Fe_2}\cdot7PF_6\cdot Cl$ (70%) as a dark green solid. Complete anion exchange requires repeated reprecipitation from aqueous NH_4PF_6 solution. ^{1}H NMR: δ=1.39 (t, J=8 Hz, 12H), 1.41 (t, J=8 Hz, 12H), 2.1 (m, overlaps with residual solvent, 16H), 3.65–3.96 (m, 16H), 5.97 (s, 4H), 6.58 (d, J=5 Hz, 4H), 6.65 (d, J=5 Hz, 4H), 6.82 (t, J=5 Hz, 4H), 6.87 (t, J=5 Hz, 4H), 7.67 (t, J=6 Hz, 8H), 8.12 (d, J=6 Hz, 4H), 8.33 (d, J=6 Hz, 4H), 8.40 (s, 4H), 8.49 (s, 4H), 9.20 (br s, 4H), 9.28 (br s, 4H), 9.73 (br s, 4H); MS (FAB+): *m/z* (%): 3654 (2) [M^+-Cl], 3544 (18) [M^+-PF_6], 3508 (8) [$M^+-Cl-PF_6$], 3399 (15) [M^+-2PF_6], 3363 (8) [$M^+-Cl-2PF_6$); elemental analysis calcd (%) for $C_{120}H_{112}F_{42}ClN_{24}P_7S_8Os_2Fe_2$: C 39.06, H 3.04, N 9.11; found: C 38.87, H 3.27, N 9.05.

© 2003 Wiley-VCH Verlag GmbH & Co. KGaA, Weinheim

Complex [{Fe(1)}$_4$][PF$_6$]$_8$ (Fe$_2$Fe$_2$): Compound **1** (200.0 mg, 0.37 mmol) and iron(II)tetrafluoroborate hexahydrate (0.13 mg, 0.37 μmol) were placed in a 50 mL round-bottomed flask. Upon addition of nitromethane (40 mL), the solution rapidly turned dark green. Stirring was continued at room temperature for 3 days (until no further change by TLC). Nothing precipitated by addition of TBAC, so the nitromethane was removed, and the was residue triturated with acetonitrile and diluted by an equal volume of toluene. The green solid was collected and purified by column chromatography (silica, MeOH/NH_4Cl (2M)/$MeNO_2$ 7:2:1). The green band was collected and the product recovered by addition of NH_4PF_6 followed by removal of the volatile organic solvents under reduced pressure and filtration. Reprecipitation with aqueous NH_4PF_6 solution and drying yielded 240 mg of **Fe$_2$Fe$_2$**·7PF$_6$·Cl (18%) as a dark green solid. Complete anion exchange requires repeated reprecipitation from aqueous NH_4PF_6 solution. ^{1}H NMR: $\delta = 1.41$ (t, $J = 8$ Hz, 24H), 2.1 (m, overlaps with residual solvent, 16H), 3.75 (m, 16H), 5.73 (s, 4H), 6.46 (d, $J = 5$ Hz, 8H), 6.82 (t, $J = 5$ Hz, 8H), 7.68 (t, $J = 6$ Hz, 8H), 8.20 (d, $J = 6$ Hz, 8H), 8.54 (s, 8H), 8.89 (br s, 4H), 9.00 (s, 8H); MS (FAB+): *m/z* (%): 3385 (25) [M^+−Cl], 3275 (85) [M^+−PF$_6$], 3289 (45) [M^+−Cl−PF$_6$), 3130 (40) [M^+−2PF$_6$], 3095 (40) [M^+−Cl−2PF$_6$], 2985 (10) [M^+−3PF$_6$], 2950 (14) [M^+−Cl−3PF$_6$]; elemental analysis calcd (%) for $C_{120}H_{112}ClF_{42}N_{24}P_7S_8Fe_4$: C 42.14, H 3.30, N 9.83; found: C 42.95, H 3.55, N 9.80.

Acknowledgement

We wish to thank MIUR, CNR (Agenzia 2000) for financial support. D.M.B. is grateful to the EU HCM program for a Marie Curie Fellowship.

[1] a) J.-M. Lehn, *Supramolecular Chemistry. Concept and Perspectives*, VCH, New York, **1995**, Chapter 8; b) J.-M. Lehn, *Supramolecular Chemistry. Concept and Perspectives*, VCH, New York, **1995**, p. 200.; c) V. Balzani, M. Venturi, A. Credi, *Molecular Devices and Machines*, Wiley-VCH, Weinheim, **2003**.

[2] a) A. J. Bard, *Integrated Chemical Systems—A Chemical Approach to Nanotechnology*, Wiley, New York, **1994**.; b) *Molecular Electronics: Science and Technology* (Eds.: A. Aviram, M. Ratner), The New York Academy of Sciences, New York, **1998**.

[3] a) J.-M. Lehn, *Proc. Nat. Acad. Sci.*, **2002**, *99*, 4763, and references therein; b) J.-M. Lehn, *Science*, **2002**, *295*, 2400.

[4] a) *Comprehensive Supramolecular Chemistry, Vol. 9* (Eds.: J. L. Atwood, J. E. D. Davies, D. D. MacNicol, F. Vögtle, J.-M. Lehn), Pergamon, Oxford, **1996**; b) D. L. Caulder, K. N. Raymond, *Acc. Chem. Res.* **1999**, *32*, 975; c) S. Leininger, B. Olenyuk, P. J. Stang, *Chem. Rev.* **2000**, *100*, 853; d) A. von Zelewsky, O. Mamula *J. Chem. Soc. Dalton Trans.* **2000**, 219; e) M. Fujita, K. Umemoto, M. Yoshizawa, T. Kusukawa, K. Birhada, *Chem. Commun.* **2001**, 509; f) J.-P. Collin, C. Dietrich-Bucheker, P. Gavina, M. C. Jimenez-Molero, J.-P. Sauvage, *Acc. Chem. Res.* **2001**, *34*, 477; g) S. Encinas, L. Flamigni, F. Barigelletti, E. C. Constable, C. E. Housecroft, E. R. Schofield, E. Figgemeier, D. Fenske, M. Neuburger, J. G. Vos, M. Zehnder, *Chem. Eur. J.* **2002**, *8*, 137; h) E. C Constable, O. Eich, D. Fenske, C. E. Housecroft, L. A. Johnston, *Chem. Eur. J.* **2000**, *6*, 4364; i) E. C. Constable, *Chem. Commun.* **1997**, 1073.

[5] a) G. S. Hanan, D. Volkmer, U. S. Schubert, J.-M. Lehn, G. Baum, D. Fenske, *Angew. Chem.* **1997**, *109*, 1929; *Angew. Chem. Int. Ed. Engl.* **1997**, *36*, 1842; b) O. Waldmann, J. Hassmann, P. Müller, G. S. Hanan, D. Volkmer, U. S. Schubert, J.-M. Lehn, *Phys. Rev. Lett.* **1997**, *78*, 3390; c) J. Rojo, F. J. Romero-Salguero, J.-M. Lehn, G. Baum, D. Fenske, *Eur. J. Inorg. Chem.* **1999**, 1421; d) E. Breuning, M. Ruben, J.-M. Lehn, F. Renz, Y. Garcia, V. Ksenofontov, P. Gütlich, E. Wegelius, K. Rissanen, *Angew. Chem.* **2000**, *112*, 2563; *Angew. Chem. Int. Ed.* **2000**, *39*, 2504.

[6] M. Ruben, E. Breuning, M. Barboiu, J.-P. Gisselbrecht, J.-M. Lehn, *Chem. Eur. J.* **2003**, *9*, 291.

[7] a) U. Ziener, E. Breuning, J.-M. Lehn, E. Wegelius, K. Rissanen, G. Baum, D. Fenske, G. Vaughan, *Chem. Eur. J.* **2000**, *6*, 4132; b) E. Breuning, U. Ziener, J.-M. Lehn, E. Wegelius, K. Rissanen, *Eur. J. Inorg. Chem.* **2001**, 1515.

[8] a) V. Smith, J.-M. Lehn, *Chem. Commun.* **1996**, 2733; b) J.-M. Lehn, *Chem. Eur. J.* **2000**, *6*, 2097; c) D. P. Funeriu, J.-M. Lehn, K. M. Fromm, D. Fenske, *Chem. Eur. J.* **2000**, *6*, 2103.

[9] D. M. Bassani, J.-M. Lehn, K. Fromm, D. Fenske, *Angew. Chem.* **1998**, *110*, 2534; *Angew. Chem. Int. Ed.* **1998**, *37*, 2364.

[10] a) B. Hasenknopf, J.-M. Lehn, G. Baum, B. O. Kneisel, D. Fenske, *Angew. Chem.* **1996**, *108*, 1987; *Angew. Chem. Int. Ed. Engl.* **1996**, *35*, 1838; b) B. Hasenknopf, J.-M. Lehn, N. Boumediene, A. Dupont-Gervais, A. Van Dorsselaer, B. Kneisel, D. Fenske, *J. Am. Chem. Soc.* **1997**, *119*, 10956.

[11] A. Juris, V. Balzani, F. Barigelletti, S. Campagna, P. Belser, A. von-Zelewsky, *Coord. Chem. Rev.* **1988**, *84*, 85.

[12] S. Serroni, S. Campagna, R. Pistone Nascone, G. S. Hanan, G. J. E. Davidson, J.-M. Lehn, *Chem. Eur. J.* **1999**, *5*, 3523.

[13] E. M. Kober, J. V. Caspar, B. P. Sullivan, T. J. Meyer, *Inorg. Chem.* **1988**, *27*, 4587.

[14] a) V. Balzani, A. Juris, M. Venturi, S. Campagna, S. Serroni, *Chem. Rev.* **1996**, *96*, 759; b) F. Scandola, C. Chiorboli, M. T. Indelli, M. A. Rampi, in *Electron Transfer in Chemistry, Vol. 3* (Ed.: V. Balzani), Wiley-VCH, Weinheim, **2001**, p. 337.

[15] a) A. Credi, V. Balzani, S. Campagna, G. S. Hanan, C. R. Arana, J.-M. Lehn, *Chem. Phys. Lett.* **1995**, *243*, 105; b) P. Ceroni, A. Credi, V. Balzani, S. Campagna, G. S. Hanan, C. R. Arana, J.-M. Lehn, *Eur. J. Inorg. Chem.* **1999**, 1409.

[16] a) T. J. Meyer, *Pure Appl. Chem.* **1986**, *58*, 1193; b) G. R. Crosby, *Acc. Chem. Res.* **1975**, *8*, 231.

[17] a) M. Maestri, N. Armaroli, V. Balzani, E. C. Constable, A. M. W. Cargill Thompson, *Inorg. Chem.* **1995**, *34*, 2759; b) J.-P. Sauvage, J. P. Collin, J. C. Chambron, S. Guillerez, C. Coudret, V. Balzani, F. Barigelletti, L. De Cola, L. Flamigni, *Chem. Rev.* **1994**, *94*, 993; c) S. Encinas, L. Flamigni, F. Barigelletti, E. C. Constable, C. E. Housecroft, E. R. Schofield, E. Figgemeier, D. Fenske, M. Neuburger, J. G. Vos, M. Zehnder, *Chem. Eur. J.* **2002**, *8*, 137; d) F. Loiseau, R. Passalacqua, S. Campagna, M. I. J. Polson, Y.-Q. Fang, G. S. Hanan, *Photochem. Photobiol. Sci.* **2002**, *1*, 982.

[18] a) A. El-ghayoury, A. Harriman, A. Khatyr, R. Ziessel, *Angew. Chem.* **2000**, *112*, 191; *Angew. Chem. Int. Ed.* **2000**, *39*, 185; b) A. El-ghayoury, A. Harriman, A. Khatyr, R. Ziessel, *J. Phys. Chem. A* **2000**, *104*, 1512; c) Y.-Q. Fang, G. S. Hanan, F. Loiseau, R. Passalacqua, S. Campagna, H. Nierengartner, A. Van Dorsselaer, *J. Am. Chem. Soc.*, **2002**, *124*, 7912; d) R. Passalacqua, F. Loiseau, S. Campagna, Y.-Q. Fang, G. S. Hanan, *Angew. Chem.* **2003**, *115*, 1645; *Angew. Chem. Int. Ed.* **2003**, *42*, 1607.

[19] P. Chen, T. J. Meyer, *Chem. Rev.* **1998**, *98*, 1439.

[20] a) V. Balzani, F. Scandola, *Supramolecular Photochemistry*, Horwood, Chichester, **1991**.

[21] a) H. Berglund Baudin, J. Davidsson, S. Serroni, A. Juris, V. Balzani, S. Campagna, L. Hammarström, *J. Phys. Chem. A*, **2002**, *106*, 4312; b) J. Andersson, T. Polivka, V. Sundström, F. Puntoriero, S. Serroni, S. Campagna, unpublished results

[22] At this point, two issues warrant further comments. The first deals with the question whether the proper way to discuss the photophysical properties of the molecular grids is the multicomponent, supramolecular approach used here, in which excitation is considered to be localized on individual subunits, or a delocalized approach, treating excitation as delocalized over the whole molecule. In the latter case, of course, energy-transfer processes would lose their meanings. Localization of the redox processes, as clearly indicated by the electrochemical experiments (see later) and the straightforward assignment of absorption features to specific subunits of the grids strongly support the supramolecular approach. The second issue is related to the ultrafast energy transfer: considering the intrinsic lifetimes of Ru^{II} and Os^{II} polypyridine complexes (usually in the nanosecond timescale, see refs. [11,14]) organized structures like grids, ladders, and racks based on these building blocks could exhibit highly efficient energy- and electron-migration processes even for systems containing tens of metal centers, if bridging ligands similar to **1** are used and suitable energetic requirements are followed.

[23] a) G. S. Hanan, U. S. Schubert, D. Volkmer, E. Rivière, J.-M. Lehn, N. Kyritsakas, J. Fischer, *Can. J. Chem.* **1997**, *75*, 169; b) G. S.

 © 2003 Wiley-VCH Verlag GmbH & Co. KGaA, Weinheim

Hanan, C. R. Arana, J.-M. Lehn, G. Baum, D. Fenske, *Chem. Eur. J.* **1996**, *2*, 1292.
[24] G. Denti, S. Campagna, L. Sabatino, S. Serroni, M. Ciano, V. Balzani; *Inorg. Chem.* **1990**, *29*, 4750.
[25] a) A. A. Vlceck, *Coord. Chem. Rev.* **1982**, *43*, 39; b) A. Mamo, I. Stefio, M. F. Parisi, A. Credi, M. Venturi, C. Di Pietro, S. Campagna, *Inorg. Chem.* **1997**, 36, 5947; c) M. Marcaccio, F. Paolucci, C. Paradisi, S. Roffia, C. Fontanesi, L. J. Yellowlees, S. Serroni, S. Campagna, G. Denti, V. Balzani, *J. Am. Chem. Soc.* **1999**, *121*, 10081, and references therein.
[26] It could be tentatively suggested that the LUMO π^* orbital of the bridging ligand **1** in $\mathbf{Os_2Fe_2}$ can receive significant contributions also from the peripheral bipyridine moiety coordinating the Fe^{II} center, in addition to the more important contribution from the pyrimidine subunit, because the extent of backbonding from Os^{II} is greater than from the Fe^{II}, leading to electronic asymmetry of the bridge. As a consequence, the sites of the reduction processes of $\mathbf{Os_2Fe_2}$, that is, the π^* **1** orbitals, should be less localized on the pyrimidine ring than in the other grids (they extend significantly towards one of the chelating sites and the contribution of the pyrimidine ring is weaker). With this hypothesis, on looking at the structure of the $\mathbf{Os_2Fe_2}$ grid, it is apparent that the asymmetry of the reduction sites leads to an increased distance between them (i.e., while in symmetric grids the reduction sites are in a first approximation two pyrimidine rings facing one another, in the "asymmetric" $\mathbf{Os_2Fe_2}$ grid the reduction sites would involve the iron-coordinated terpy-like moieties of each parallel bridging ligand) and therefore can justify the coalescence of the two reduction processes.
[27] D. M. Bassani, J.-M. Lehn *Bull. Soc. Chim. Fr.* **1997**, *134*, 897.
[28] J. N. Demas, G. A. Crosby, *J. Phys. Chem.* **1971**, *75*, 991.
[29] R. S. Lumpkin, T. J. Meyer, *J. Phys. Chem.* **1986**, *90*, 5307.

Received: August 13, 2003 [F5441]

© 2003 Wiley-VCH Verlag GmbH & Co. KGaA, Weinheim